ADVANCED FUNCTIONAL MATERIALS
www.afm-journal.de

Highly Extensible Bio-Nanocomposite Films with Direction-Dependent Properties

By *Akhilesh K. Gaharwar, Patrick Schexnailder, Vikas Kaul, Ozan Akkus, Dmitri Zakharov, Soenke Seifert,* and *Gudrun Schmidt**

The structure and mechanical properties of bio-nanocomposite films made from poly(ethylene oxide) (PEO) that is physically cross-linked with silicate nanoparticles, Laponite, are investigated. Direction-dependent mechanical properties of the films are presented, and the effect of shear orientation during sample preparation on tensile strength and elongation is assessed. Repeated mechanical deformation results in highly extensible materials with preferred orientation and structuring at the nano- and micrometer scales. Additionally, in vitro biocompatibility data are reported, and NIH 3T3 fibroblasts are observed to readily adhere and proliferate on silicate cross-linked PEO while maintaining high cell viability.

1. Introduction

Nature offers inspiration for creating high-performance biomaterials from soft polymer and hard nanoparticle components. Successful design and function of such advanced biomaterials often requires the nanoparticles to be exfoliated in the polymer matrix, and the self-assembly of supramolecular structures to be controlled. Biology offers the best models for strategies on how to reproduce the properties of high-performance materials, such as bone, nacre, and silk.[1–5] As we try to mimic the biological design using a combination of materials, new nanocomposite biomaterials are being developed with physical properties that far exceed those of conventional synthetic polymer composites. However, the complexity, perfection, and efficiency of nature are not easily matched. For example, nacre is made under ''mild'' conditions and is 1000 times as tough as the organic soft and inorganic hard phases of which it is composed.[6,7] Bone has a hierarchical structure with mechanical properties that ideally last for a lifetime.[8] Nevertheless, some authors recently reported that the perfect assembly of particles at the nanoscale is not absolutely necessary to obtain macroscopic ordered structures that have strength and stiffness comparable to natural materials.[6,9–12]

Hierarchically ordered nanocomposites from polymer and silicate nanoplatelets have been the subject of much research, and comprehensive reviews are available.[13–16] Strong specific interactions between silicate surfaces and polymer molecules combined with new fabrication techniques allow the assembly of supramolecular structures on all length scales.[16–18] Besides covalent bonding, physical cross-linking via hydrogen bonding, van der Waals and ionic interactions are responsible for inducing high mechanical strength and extensibility,[19] properties that can be similar to those of Kevlar[20,21] and steel.[22] While small amounts of silicate nanoparticles dramatically change the physical properties of polymers,[13–16] high amounts of silicate can lead to ultrastrong materials with hierarchical structures and properties that may approach the theoretically calculated maximum.[9,10]

One of the main difficulties associated with the fabrication of mechanically superior nanocomposites is the uniform dispersion of polymer and nanoparticles and their positioning on nanometer scales. In order to overcome these problems, researchers have used processing technologies, such as the layer-by-layer technique,[23] to form nanometer-sized mortar and brick structures that resemble nacre.[7,10] Ultrahigh tensile strength is achieved through efficient load transfer between polymer and silicate nanoparticles.[7,10] Other creative and new approaches were able to overcome the thermodynamic and kinetic barriers of nanoparticle dispersion via solvent exchange.[9] The strong adhesion between the silicate and polymer microdomains and the formation of a percolative network can induce thermotropic liquid crystalline behavior in addition to mechanical strength.[9] Other fabrication techniques include the continuous self-assembly and polymerization of silica, surfactant, and monomers into nacrelike nanolaminated coatings, which was achieved by Sellinger et al.[6] Evaporation-induced partitioning and self-assembly resulted in the simultaneous organization of thousands of layers at once.[6] Finally, Dundigalla et al. have used simple spreading and drying techniques to obtain highly ordered mortar and brick structures in films made from nanocomposite hydrogels.[24]

[*] Prof. G. Schmidt, A. K. Gaharwar, P. Schexnailder, V. Kaul, Prof. O. Akkus
Purdue University
Weldon School of Biomedical Engineering
West Lafayette, IN, 47907 (USA)
E-mail: gudrun@purdue.edu
Dr. D. Zakharov
Purdue University
Birck Nanotechnology Center
West Lafayette, IN, 47907 (USA)
Dr. S. Seifert
Advanced Photon Source
Argonne National Laboratory
Argonne, IL, 60439 (USA)

DOI: 10.1002/adfm.200901606

The evolving nano- and biotechnologies offer synergistic opportunities to optimize and refine complex materials made from silicate and polymer. Biomaterials are being developed by scientists that work at the interdisciplinary boundaries of life sciences and engineering. The control of chemical, physical, and biological properties in silicate-based nanocomposites can not only mimic the performance of natural materials, but also has the potential to repair human tissues. For example, silicate has already been observed to promote tissue repair, as early studies have shown that silicon normally present in vivo is essential in the formation of cartilage and bone.[25,26] More recent studies found that the dissolution products of bioactive glass (surface active glass ceramics containing SiO_2, CaO, P_2O_5, etc.) enhance cell proliferation and gene expression.[27,28] These results, and many other findings from literature, demonstrate the ability of silicate to enhance cell growth,[28] thus offering inspiration for creating new biomaterials.

With a long-term goal of developing a model polymer–silicate nanocomposite with controlled cell adhesion for biomedical applications, we have chosen silicate nanoplatelets (Laponite) as reversible physical cross-linkers to poly(ethylene oxide) (PEO) because Laponite exfoliates easily, and the polymer readily adsorbs onto the charged nanoparticle surfaces.[29,30] In this contribution, we present direction-dependent mechanical properties of films prepared from PEO crosslinked with Laponite. We assess the effect of shear orientation during sample preparation on mechanical properties with the intention of improving the strength and stiffness at the macroscopic level. We observe that mechanical deformation results in highly extensible materials that have preferred orientation at the nano- and micrometer scales. This structural alignment is supported by data from polarized microscopy and X-ray scattering experiments. Finally, cell growth studies show that cross-linking PEO with silicate nanoparticles results in biomaterials that support cell attachment, growth, and proliferation while maintaining high cell viability.

2. Results and Discussion

The directionally dependent mechanical properties of the dried nanocomposite films depend on the nano- and micrometer-sized structural features, on the PEO–Laponite interactions, and on the shear orientation induced by film preparation[31,32] and stretching. For example, the high-molecular-weight polymer ($M_w = 10^6$ g/mol PEO) that is used for making gels and then films, increases the interconnectivity between the Laponite cross-linkers compared to low M_w polymers. A high degree of connectivity between Laponite cross-linkers and PEO polymer chains leads to stronger and stiffer materials.

2.1. Structures of Films

For a better interpretation of the mechanical testing data, we briefly discuss the structure of the silicate cross-linked PEO films. In previous work, we have shown that over nanometer-length scales, polymer-covered silicate platelets will aggregate and orient in bundles while the interconnecting polymer chains remain amorphous.[24,32] On micrometer-length scales, highly oriented multilayers are formed due to polymer phase separation and shear orientation during the film preparation process. The top film surface is smooth while the side surface is layered. The exact film preparation process needs to be followed to reproduce layered structures.[24] If the film preparation procedure is not followed precisely, films with other structures may be generated. Figure 1a shows a scanning electron microscopy (SEM) image of a representative film as seen from the side. The multilayered structures seen by SEM indicate that we can reproduce films with the same structures and morphologies described previously. Therefore the mechanical testing data presented in this work can be correlated with the film structures reported earlier.[24]

When silicate cross-linked PEO films are subjected to uniaxial deformation, the elongation and unidirectional stiffness of the film increases, and the bending and knotting properties are enhanced (Fig. 1b). Birefringence is observed under crossed polarizers after strain-induced alignment (stretching, Fig. 1c). The interface between the stretched and unstretched parts of the film can be identified clearly under crossed polarizers. The sharp interface corresponds to the grip location. The birefringent part of the film is a result of shear-induced alignment and crystallization and suggests the presence of highly oriented polymer chains and possible aligned nanoparticles. The uniform color of birefringence and the lack of large polymer crystallites that are usually visible for

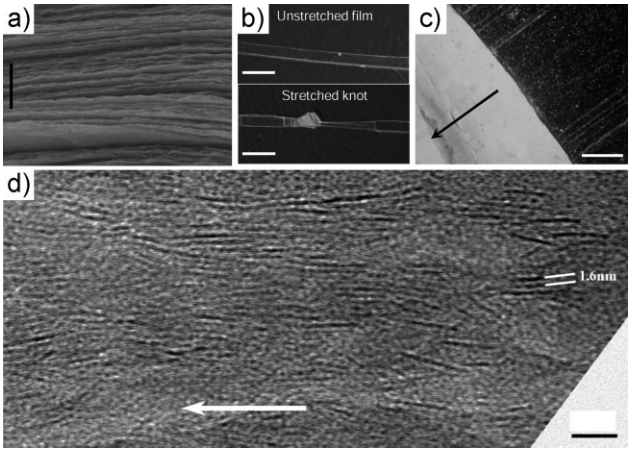

Figure 1. Structures of bio-nanocomposite films. a) SEM image of a fractured multilayer film as seen from the side (*YZ* plane). Several micrometer-thick sublayers are visible. Scale bar: 2 μm. b) Top: transparent and flexible 70 μm thick nanocomposite film. Bottom: a part of the film was stretched during knotting (Scale bar = 1 cm). c) Cross-polarized microscopy image showing birefringence caused by strain-induced alignment during tensile testing. The interface between the stretched (bright and birefringent) and unstretched (dark) region indicates the previous location of the grip. The stretch direction was perpendicular to the birefringent interface as indicated by the arrow. The birefringent part of the film is a result of shear-induced alignment and polymer crystallization. The uniform color of birefringence indicates that the polymer chains must be aligned. The dark (black) part of the film was not stretched. The lack of birefringence indicates that the cross-linked polymer is either amorphous, or birefringence is not sensitive enough to measure orientation characteristics caused by sample preparation (Scale bar: 50 μm). d) TEM image of a stretched nanocomposite film as seen from the side (*YZ* plane). Arrow indicates spreading direction. Nanoplatelets are uniformly arranged in layered structures along the spreading direction. Intercalated particles are evident with a 1.6 ± 0.1 nm spacing between platelets (Scale bar = 10 nm).

PEO, suggest no individual domains of preferred orientation of the polymer or nanoparticle; nevertheless, the polymer chains are aligned in the stretching direction. The dark (black) part of the film shown in Figure 1c was not stretched. The lack of birefringence indicates that the cross-linked polymer is either amorphous, or birefringence is not sensitive enough to measure orientational characteristics caused by sample preparation (spreading and drying). Lines observed within the dark areas of the film come from manual spreading and indicate inhomogeneities in film thickness.

Birefringence usually originates from the orientation of anisotropic structures such as elongated polymer chains, from oriented or crystallized polymer domains or from aligned nanoparticles. With multiple components present in one sample, we cannot easily distinguish between the contributions of each of these components. However, our observations show that birefringence disappears when the stretched films are heated above the polymer melting temperature (PEO $\sim 60\,^{\circ}$C). While aligned polymer chains cause birefringence at room temperature, once the polymer melting temperature is reached, these polymer chains will randomize into polymer coils that are not birefringent. This observation suggests that the birefringence (top view of film) must be dominated by polymer orientation rather than by silicate nanoparticle orientation.

Birefringence of the stretched and unstretched film side view (not shown here) does not disappear when the film is heated. A representative transmission electron microscopy (TEM) image of the stretched film (Fig. 1d, side view of film) shows the dispersion morphology of silicate nanoplatelets within the PEO matrix. Closely packed nanoplatelets (side view), with an intercalated distance of $\sim 1.6 \pm 0.1$ nm are visible. TEM images of both, unstretched and stretched films, show similar morphology; however the image of the stretched film has highly ordered platelets within a domain, or area, of several hundred square nanometers (see Fig. 1d). TEM images of the unstretched film (not shown here) have domains that are less ordered with regard to each other. The average intercalated distance between silicate platelets, as seen by TEM, does not change before and after stretching.

2.2. Direction-Dependent Mechanical Properties

To evaluate the effect of shear orientation (spreading) during film preparation on the mechanical strength of the dried films, samples were tested i) along the original spreading direction (*Z*) and ii) perpendicular to the spreading direction (*X*). Representative stress–strain curves are shown in Figure 2a. Overall, the results show that the mechanical properties are direction-dependent, suggesting that the spreading direction during film preparation significantly influences the mechanical strength and elongational capability of the dried film.

Films stretched in the *Z* direction show mean tensile moduli of ~23 MPa, mean yield strengths of ~17 MPa, and a maximum elongation of about ~160% (Fig. 2a). Films stretched along the *X* direction show similar tensile moduli (~22 MPa) and yield

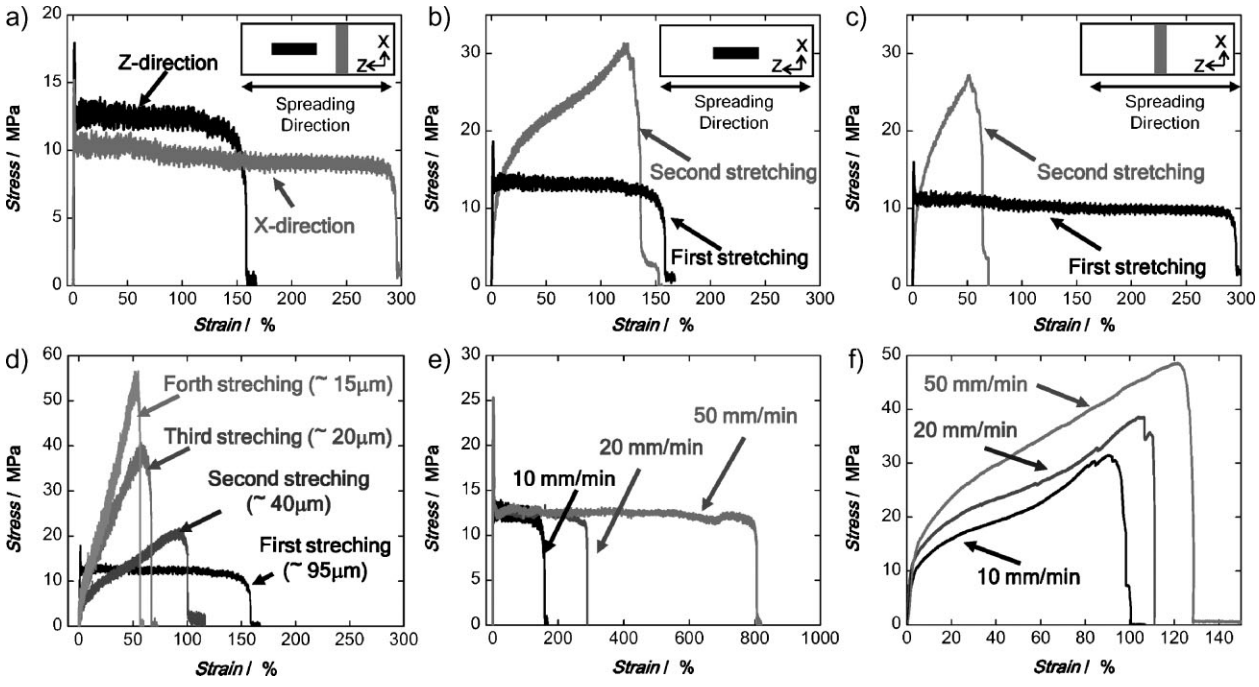

Figure 2. Directionally dependent mechanical properties of nanocomposites. a) Representative stress–strain curves from unstretched films in different directions. Inset shows a schematic representation of the film with definitions of film planes and locations of cut test specimens. The spreading direction during all sample preparations was "Z." b,c) Films cut and stretched in the *Z* direction exhibit higher yield stresses and lower elongations than films cut and stretched in the *X* direction. b) After a second stretching experiment, stress–strain curves show enhanced mechanical strength due to strain-induced alignment. Samples stretched a second time in the *Z* direction show higher moduli and strength compared to their first stretched counterparts. c) Samples that were stretched in the *X* direction show much higher elongation than those stretched in *Z* (b). d) Repeated stretching leads to higher tensile strength. e) Increased strain rates lead to increased elongation and strength. e,f) First stretching experiments (e) are compared to second stretching experiments (f).

Final page numbers not assigned

strengths (~15 MPa); however, the elongation is nearly twice as high, ~300%, when compared to films stretched along the *Z* direction. Such differences must be related to the shear orientation of the cross-linked polymer network during sample preparation (spreading). If we assume that the shear orientation in the *X* direction caused by spreading is near zero, then the elongation caused by spreading alone is estimated to be 140% (300–160% = 140%).

To investigate the influence of repeated stretching on the mechanical properties, we performed a series of repeated tensile tests (Fig. 2b–d). After stretching, all films appear strongly birefringent under crossed polarizers (similar to films shown in Fig. 1), and the overall thickness decreased from ca. ~95 to ~45 μm for films stretched in *Z* direction and to ~20 μm for films stretched in *X* direction. The average film width did not change substantially. Although the SEM image in Figure 1 shows multilayered microstructures, the films did not delaminate during the mechanical testing experiments. After the first experiment (first stretching), films were cut and subjected to repeated tensile testing. We will refer to these experiments as "second stretching," "third stretching," etc. Figure 2b–d summarize and compare representative stress–strain curves from both experiments. The films that were stretched a second time in the *Z* and *X* directions (Fig. 2b and c) exhibited twice as high tensile strengths (~32 and ~28 MPa, respectively) when compared to their "first stretched" counterparts. Subsequent stretching of films in the *Z* direction resulted in higher tensile strengths (Fig. 2d). Increased strain rates led to increased elongation and strength (Fig. 2e,f), especially when first stretching experiments were compared to second stretching experiments. Overall, multiple stretching did not significantly affect the ductility of the nanocomposite films. In addition to elongation, both the films (unstretched and stretched) could withstand torsion, tearing, bending, and knotting (as shown in Fig. 1). Our results have some similarity to the work published by Podsiadlo et al. who have demonstrated that the layer-by-layer assembly of polymer and natural Montmorillonite clay results in ultrastrong and stiff films that have similar structures compared to our materials.[10]

In contrary to non-cross-linked pure PEO, the silicate cross-linked nanocomposite films presented here show higher elongation at greater stain rates (Fig. 2e). The elongation of the films seems to be directly proportional to the applied stain rate. When the stain rate is increased from 10 to 50 mm/min (a fivefold increase), we also observed a fivefold increase in percent elongation (from 160 to 800%). A second stretching of the films showed additional stain-rate-dependence (Fig. 2f).

Overall, the combination and formulation of silicate nanoparticles with PEO synergistically allows us to combine advantageous polymer properties of PEO with those of silicate nanoparticles (Laponite) to develop new biomaterials that cannot be made from either component alone. For example, reference Laponite films remain brittle while reference PEO films easily dissolve in water and melt above ca. 60 °C.

2.3. Nanometer Structural Orientation of Films as Tested by X-Ray Scattering

Wide-angle X-ray scattering (WAXS) and small-angle X-ray scattering (SAXS) were used to evaluate the nanometer structural orientation present in the a) as-prepared (unstretched) films, and films that have undergone the "second stretching" experiment in b) *X* direction and c) in *Z* direction. Results presented in Figure 3, show 2D WAXS and SAXS spectra, along with averaged SAXS scattering intensities versus momentum transfer, *q*, for the three types of films.

Although the data presented in Figure 2 (mechanical testing) suggested that some degree of orientation must be present after sample preparation for directionally dependent mechanical properties to occur, polarized microscopy (Fig. 1c) as well as SAXS (Fig. 3d–f) cannot detect anisotropic structural orientation in the as-prepared films. The 2D SAXS spectra of the as-prepared films are isotropic which indicates the presence of randomly oriented nanometer structures. No scattering anisotropy was observed for these as-prepared films (Fig. 3). The stretched films, however, show highly anisotropic SAXS patterns, which indicate alignment of polymer chains and silicate platelets.[33,34] Films stretched in the *Z* direction, particularly, suggest the formation of PEO crystallites within lamellar PEO-LRD structures. Support of PEO crystallization under deformation can be found in a recent article by Wang et al., which reports on the crystallization of PEO when the polymer is in a confined environment.[35]

The scattering intensity as function of *q* was calculated from the 2D SAXS patterns in meridional and equatorial directions (*X* and *Z* directions; Fig. 3g–i). The scattering of the as-prepared films measured in the *X* and *Z* directions are nearly identical. The degree of anisotropy in the stretched films can be estimated from the extent of bifurcation in *X* and *Z* intensities at low *q*. A maximum in intensity observed at high *q* ($q = 0.354$ Å^{-1}) corresponds to a characteristic length of ~1.78 nm and correlates with the intercalated distance obtained from TEM images (Fig. 1). This distance is related to the 001 basal plane spacing between PEO-covered Laponite platelets. The maximum is more pronounced when films are stretched in *Z* direction than in *X* direction. A pure Laponite film consisting of layered platelets only, has an average distance between platelets of ~1.34 nm.[35] The increase in interlayer distance between pure Laponite films and PEO/Laponite films is ~0.44 nm, which corresponds to the adsorbed and intercalated polymer.

While microscopy, such as TEM, images discrete sections of a sample, the SAXS scattering techniques used here average over the sample volume that the beam penetrates. Thus, TEM images individual silicate nanoplatelets within their immediate environment and within larger size domains. SAXS scattering on the contrary, averages over a volume of possibly several domains. This averaging leads to a "peak" in SAXS scattering intensity when averaging is done over a volume of domains that are highly oriented in the same direction (Fig. 3h). SAXS shows "no peak," when averaging over a volume of less oriented domains. Thus the presence of a SAXS peak in the high *q* range (which detects nanometer structures) suggests an increased degree of order after stretching. In the low *q* range (which detects larger structures, several 100 nm in size), SAXS data suggest that the degree of order might decrease after stretching (Fig. 3g). This effect could be related to a sliding and/or tearing of domains during stretching as the stretched film becomes thinner.

WAXS was used to evaluate crystallinity. The 2D WAXS pattern (Fig. 3a) from the as-prepared films shows two diffraction rings, which indicate random orientation of nanometer structures. The

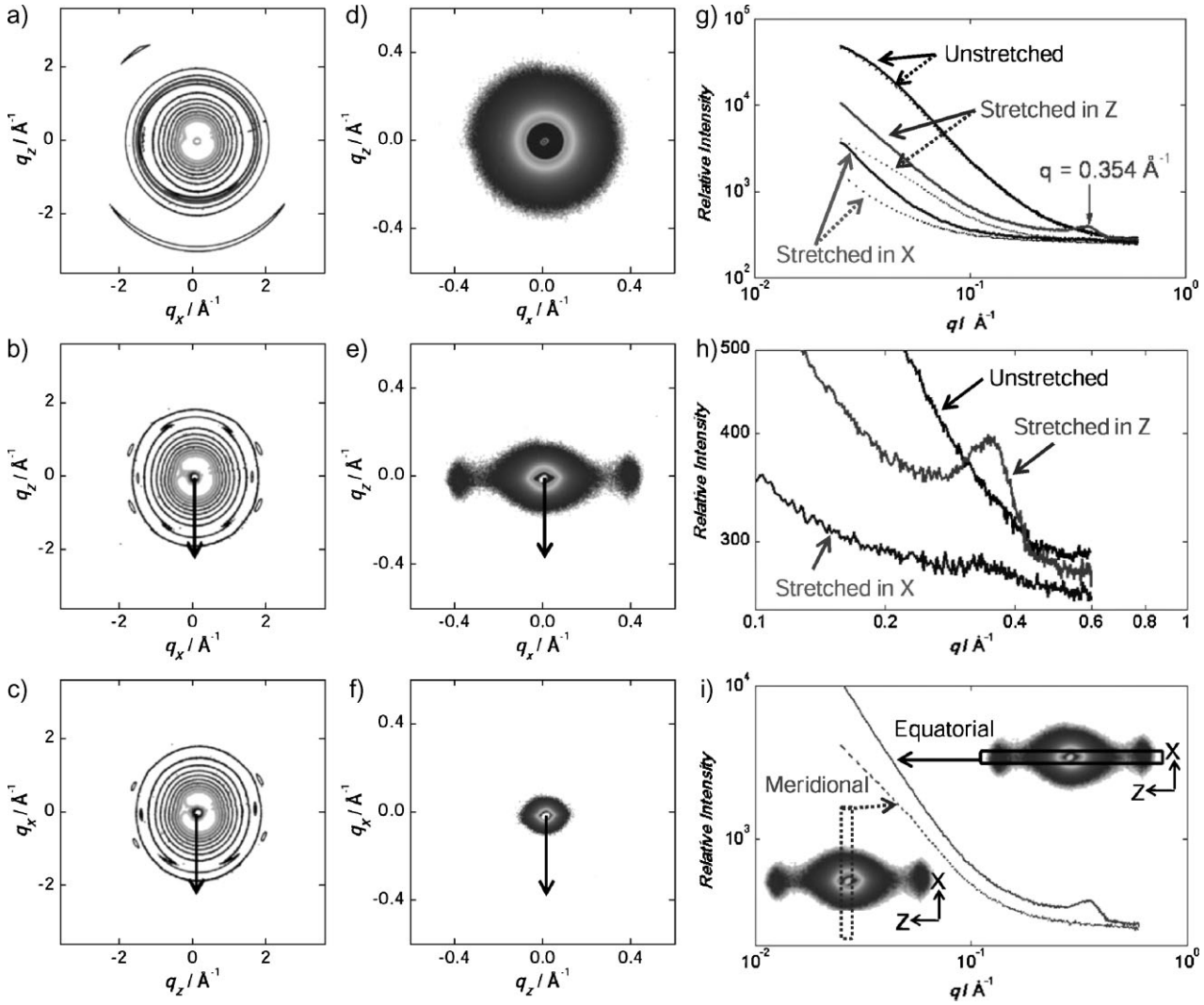

Figure 3. Structural alignment in nanocomposite films stretched in different directions. a–c) Representative 2D WAXS spectra from a) as-prepared films (unstretched), b) films after repeated stretching in the *Z* direction, and c) films after repeated stretching in the *X* direction. Arrows indicate the stretching direction of the films. The diffraction rings observed in (a) suggest random orientation of PEO-covered Laponite stacks within the *XZ* plane. The diffraction spots/arcs observed for the stretched films (b,c) suggest PEO crystallites oriented along the stretching direction. Arrows indicate the stretching direction of the films. d–f) Representative 2D SAXS spectra from d) as-prepared (unstretched) films, e) SAXS obtained after a ''second stretching'' in the *Z* direction, and f) SAXS obtained after a ''second stretching'' in the *X* direction. The anisotropic SAXS pattern after stretching the film in the *Z* direction implies significant alignment of nanometer structures (maximum at $q = 0.354$ Å^{-1}). g–i) Nanometer structural changes observed using SAXS: g) SAXS intensities as function of *q* were calculated from 2D SAXS patterns. Solid lines represent equatorial averages and dotted lines represent meridional averages of the 2D scattering. h) An enlarged section of (g) is showing a maximum at $q = 0.354$ Å^{-1} ($d = 1.78$ nm) for films stretched in the *Z* direction. i) Diagrams showing how intensities were averaged for the sample stretched in *Z* direction.

two rings at $q \sim 1.38$ Å^{-1} and $q \sim 2.45$ Å^{-1} can be attributed to the (00L) planes of polymer intercalated Laponite. No anisotropy was observed, thus the PEO crystallites that are present must be very small and randomly oriented. The diffraction patterns from stretched films (Fig. 3b,c) indicate the presence of PEO crystallites oriented along the stretching direction. The WAXS patterns from both stretched films (in *Z* and *X* directions) show six characteristic arcs that can be correlated to the monoclinic crystal structure of PEO ($a = 8.05$ Å, $b = 13.04$ Å, $c = 19.84$ Å, $\beta = 125.4°$).[36,37] The two equatorial peaks at 90° to the stretching direction (arrow) indicate the (120) crystallographic planes ($q \sim 1.38$ Å^{-1}) and the four peaks in the quadrants correspond to the (112) crystallographic planes ($q \sim 1.67$ Å^{-1}). The appearance of crystallographic peaks after stretching indicates that mechanical deformation results in alignment and crystallization of PEO chains along the stretching direction. Some of the scattering intensity coming from the (00L) basal planes of intercalated Laponite ($q \sim 1.38$ Å^{-1} and ~ 2.45 Å^{-1}) may cover the crystalline PEO peaks. The decrease in the intensity of these scattering rings after mechanical deformation might result from sliding of Laponite platelets past each other (thinner film) and from stretching of cross-linked PEO chains. Mechanical testing data showed that the film before

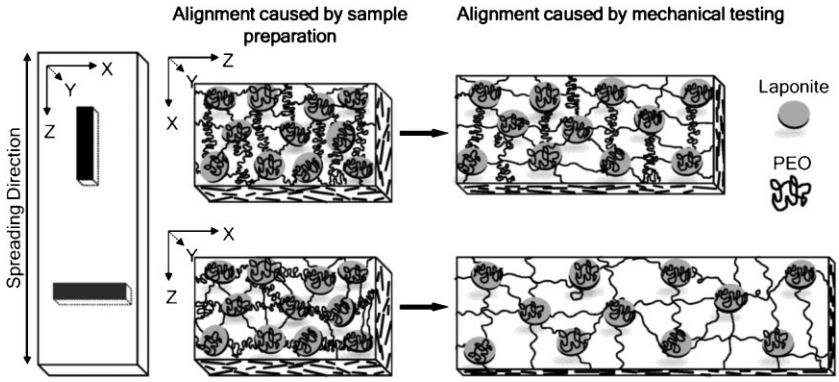

Figure 4. Schematic representation of silicate cross-linked PEO networks with alignment of PEO chains and Laponite nanoparticles. Direction-dependent mechanical properties depend on structural alignment caused by sample preparation (spreading and drying) and by mechanical testing (stretching). Sample preparation caused polymer chains to stretch in the *Z* direction (*Z* = spreading direction). In the unstretched ''as-prepared films,'' the silicate nanoparticles are oriented in *X* direction (platelet normal in *Y* direction), but are randomly distributed within the *XZ* plane. Thus mechanical testing in *Z* direction leads to greater yield strength, but lower elongation of the already aligned polymer chains. Mechanical testing in the *X* direction leads to lower yield strength, but larger elongation of the nanocomposite film.

stretching was thicker than the film after stretching; however, the film width remained the same.

Based on the above made observations and assumptions, we have developed a model that shows possible structural changes during mechanical testing of the films (Fig. 4). The model shows structural changes on a nanometer-length scale, but no changes that may occur within domains on longer length scales. The structural changes explain the direction-dependent mechanical properties that we have measured. We assumed that the polymer chains that are cross-linked between Laponite nanoplatelets build a network and that the mechanical properties are mostly influenced by this network structure. Effective load transfer between polymer and nanoparticles is a result of physical interactions, ordering, and dense packing. Our model neglects loops and dangling ends of polymer chains, as well as PEO crystallization. These structures, as well as other unknown parameters, can influence the overall mechanical properties.

During the film preparation process, which includes spreading a nanocomposite gel and drying it to form a film, polymer chains will be stretched in the *Z* direction (spreading direction), but less significantly in the *X* direction. While the film is spread, a competition between the elongation and relaxation of polymer chains[30] leads to some degree of polymer alignment in the *Z* direction (spreading direction), which is preserved in the dried film. Mechanical testing experiments deform and elongate polymer chains much more in the *X* direction than in *Z* because polymer chains are already prestretched in the *Z* direction (see Fig. 2). When we evaluated data in Figure 2a, we assumed that the shear orientation in the *X* direction caused by spreading was near zero. Thus an estimated elongation of nanostructures caused by spreading alone should be ~140% (300–160% = 140%).

The increase in tensile strength observed during the ''second stretching'' might then be related to the maximum possible elongation of polymer chains, as well as the possible rearrangement of Laponite nanoplatelets within and/or outside of PEO-intercalated Laponite layers. As the data suggested in Figure 2, the repeated elongation of the PEO chains that are cross-linked between Laponite nanoplatelets results in an overall enhancement of mechanical properties.

2.4. Cell Growth Studies

While further formulation and chemical cross-linking can optimize the material properties (mechanical) to the requirements of a specific biomedical application, here we present preliminary in vitro biocompatibility studies to show feasibility. To evaluate cell adhesion, we have cultured NIH 3T3 fibroblasts on the surface of selected films and observed that cells will grow easily on these materials and attach to the silicate cross-linked PEO surfaces more readily than to pure PEO surfaces. Figure 5a–c shows representative microscopy images of cells grown on a film surface. Cells will readily attach and grow on the surface of unstretched, as well as stretched films, and no preferential cell alignment can be observed when a stretched film is used. Cells retain their elongated, spindle-shaped morphology. The overall viability of cells remains high (~95%), as seen by the presence of only few dead cells stained with ethidium homodimer-1 and a large number of live cells stained with calcein acetoxymethyl ester (calcein AM). We have observed that fibroblast cells exhibit similarly shaped

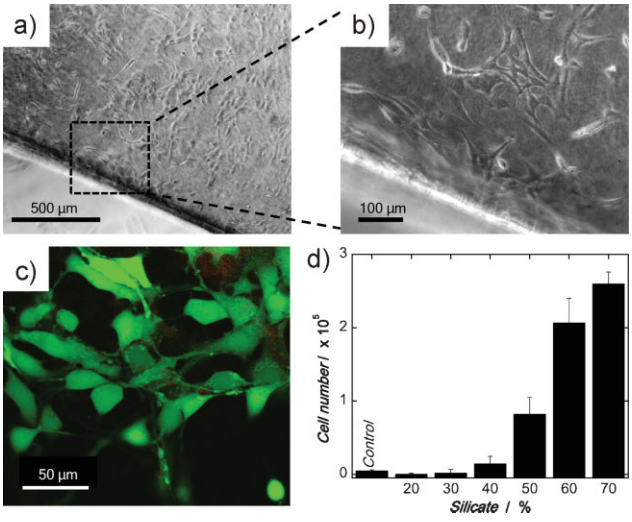

Figure 5. a,b) NIH 3T3 fibroblast cells readily adhere, grow, and proliferate on the surface of silicate cross-linked PEO films (60% silicate, 40% PEO) with an expected spindle-shaped morphology as seen with phase contrast, inverted microscopy images. c) Representative image showing that viability of cells is high (ca. 95%). A large proportion of cells are selectively labeled as living with calcein AM (green) and only a few cells were labeled as dead with ethidium homodimer-1. d) The cell number after 21 days (plateau value) from in-vitro cell cultures as function of silicate composition. Cell growth on a low binding plate has been added as control.

growth curves on the surface of nanocomposite films compared to tissue culture poly(styrene). Cell growth on a pure PEO surface (control) is considered to be zero, and cell growth on a low binding plate (control) is found to be near zero. The cell number after 21 days, which corresponds to the plateau value of the growth curve, is plotted as function of silicate composition (Fig. 5d). Although pure PEO does not support cell attachment,[38] the PEO surfaces can be made cell adhesive by the addition of silicate. Thus the cell adhesion can be precisely controlled by the amount of silicate used as cross-linker.

The silicate nanoparticles are not only able to cross-link the PEO, but are also able manifest dissolution and degradation in addition to cell adhesion properties. Our more recent studies (using fibroblast and osteoblast cells) confirm that there is a similarity between the silicate used here and bioactive glass. For example, past studies by Schwarz et al. suggested that silica from bioactive glass may act as a cross-linking agent in connective tissue,[39,40] and Hensch et al. investigated the interactions of living tissue with bioactive glasses.[41] More recent studies found that ionic dissolution products of bioactive glass indirectly enhance cell proliferation and gene expression.[27,28] Overall, many findings from the literature demonstrate the ability of silicon/silicate to enhance adhesion, differentiation, and proliferation of cells, thus offering new strategies for creating bioactive scaffolds.[42]

Our combination of PEO and silicate nanoparticles leads to bio-nanocomposite materials with a synergistic combination of chemical and physical properties that allow cell attachment and growth. Based on the high viability and significant adhesion of cells onto the surface of our films, we believe this material can be further developed for biomedical applications that require controlled cell adhesion.

3. Conclusions and Outlook

We conclude that the direction-dependent extensibility observed for our silicate cross-linked nanocomposite films depends on the shear orientation induced during spreading and stretching. Birefringence under crossed polarizers, as well as anisotropic SAXS and WAXS images indicated increased alignment of nano- and micrometer-sized structures after mechanical deformation. Strong specific interactions between nanoparticles and polymer, as well as polymer crystallization, are responsible for strain hardening and enhanced mechanical strength and extensibility. Finally, cell growth studies show that cross-linking PEO with silicate nanoparticles, Laponite, results in bio-nanocomposite materials that support cell attachment, growth, and proliferation while maintaining high cell viability. Since Laponite can be easily synthesized and dissolved under certain pH-dependent conditions,[43,44] silicate-based polymer biomaterials might be used in the future to mimic the stimulating effects of bioactive glass on cells.

4. Experimental

PEO with a molecular weight M_w of 10^6 g/mol and a molecular mass distribution of 1.5 was purchased from Polysciences Inc. Laponite (LRD) from Southern Clay Products Inc. is a synthetic Hectorite-type silicate consisting of nanoplatelets with an average diameter of 25–30 nm and a thickness of approximately 1 nm. Laponite cross-linked PEO films were prepared via gel/solution exfoliation while optimal solutions were obtained for a particular polymer silicate ratio, pH, and ionic strength [31,32]. For this work, we have prepared hydrogels composed of 2 wt.% PEO and 3 wt.% LRD at ambient temperature. Hydrogels were spread manually onto glass slides and dried at 25 °C in desiccators and subsequently under vacuum [24,32]. The composition of films after solvent evaporation was ca. 60% LRD and 40% PEO (by mass fraction). The solution pH and ionic strength in the hydrogel were held constant by adding 10^{-4} M NaOH and 10^{-3} M NaCl solvent, respectively. After drying, individual spread films have thicknesses of 7–8 μm per spread layer. Ten manually spread layers gave 70–80 μm thick films.

One representative SEM image of the side surface (*YZ* plane) is shown (Fig. 1) to indicate the ordered structures the films have. TEM was done using an FEI Titan 80/300 field-emission electron microscope with a point-to-point resolution of 2 Å at 300 kV. Samples for TEM were prepared by cryo ultramicrotome with a diamond knife at −100 °C and collected on 400 mesh carbon-coated copper grids.

Mechanical testing was done using a LE3-2 system from Test Resources Inc. LVDT output was used to control the actuator at 25 °C. Stress–strain curves were obtained by testing ~3 mm wide, ~70–80 μm thick, and ~15 mm long samples cut from films (Fig. 2). Dried films were tested 1 week after sample preparation. Grip regions were reinforced with paper to eliminate the possibility of failure at grips. Stress–strain curves were calculated for samples cut from two different directions: i) along the spreading direction (*Z*), and ii) perpendicular to spreading direction (*X*) (Fig. 2). Consecutive mechanical tests were performed after the freshly prepared samples were dried. The first one is referred to as ''first stretching,'' and the second one is referred to as ''second stretching.'' Reproducible mechanical testing data were obtained within a relative error of ca. 5% when measurements were repeated with new samples 1 week after sample preparation.

SAXS and WAXS measurements were done at Argonne National Laboratory (Advanced Photon Source) using the undulator beamline 12ID-C (11 keV). The scattering vector, q, was calibrated using a silver behenate standard at $q = 1.076\,\text{Å}^{-1}$. A q range of $0.025 < q < 0.6\,\text{Å}^{-1}$ for SAXS and $0.4 < q < 2.4\,\text{Å}^{-1}$ for WAXS was used. The 2D SAXS scattering images were corrected for spatial distortion and sensitivity of the detector, and then radially averaged to produce scattered intensity, $I(q)$, versus, q where $q = 4\pi/\lambda(\sin\theta)$.

For in vitro biocompatibility studies, NIH 3T3 mouse fibroblast cells were purchased from the American Type Culture Collection (ATCC). Cells were grown in Dulbecco's Modified Eagle's Medium (DMEM) supplemented with 10% bovine calf serum, 100 U/mL penicillin, 100 μg/mL streptomycin, and 4 mM L-glutamine. Films comprising different silicate compositions (20–70% silicate) were prepared, as described previously, for biocompatibility experiments. Films were cut into 1 cm × 1 cm squares, then briefly submerged in 70% ethyl alcohol, and allowed to dry under sterile conditions. Submersion of films in aqueous solution diminishes the mechanical properties, but does not affect cell adhesion. Films and control wells were seeded at 7 500 cells/cm^2. Media was changed every third day, and images were taken using an Olympus CKX41 phase contrast, inverted microscope. Cell number was quantified by measuring the absorbance at 490 nm using the CellTiter96 Aqueous One Solution Cell Proliferation Assay (Promega) as a metabolic indicator. Additionally, 2 μM calcein AM and 4 μM ethidium homodimer-1 (Molecular Probes) were used to label live and dead cells, respectively, to qualitatively measure the viability of cells growing on films. Calcein AM is a membrane permeable probe that intracellular esterases convert to fluorescently active calcein, therefore selectively labeling living cells. Ethidium homodimer-1 is impermeable to cell membranes [45]. However, upon rupture of the cell membrane during cell-mediated cytotoxic events, ethidium homodimer-1 interacts with DNA of dead cells and substantially increases the fluorescence of ethidium homodimer-1. Fluorescent images were taken with an Olympus FV1000 confocal microscope with excitation wavelengths of 488 and 543 nm. Representative images are shown.

Acknowledgements

Work by the authors was supported by an NSF-CAREER award 0711783 to GS and a Purdue Lynn Doctoral fellowship to PS. The authors acknowledge Avinash Dundigalla for providing the SEM image. The authors declare that they have no conflict of interest.

Received: August 26, 2009
Published online:

[1] C. Ortiz, M. C. Boyce, *Science* **2008**, *319*, 1053.
[2] W. L. Murphy, D. J. Mooney, *Nat. Biotechnol.* **2002**, *20*, 30.
[3] S. Lee, N. D. Spencer, *Science* **2008**, *319*, 575.
[4] G. Mayer, *Science* **2005**, *310*, 1144.
[5] H. Gao, B. Ji, I. L. Jager, E. Arzt, P. Fratzl, *Proc. Natl. Acad. Sci. USA* **2003**, *100*, 5597.
[6] A. Sellinger, P. M. Weiss, A. Nguyen, Y. Lu, R. A. Assink, W. Gong, C. J. Brinker, *Nature* **1998**, *394*, 256.
[7] Z. Tang, N. A. Kotov, S. Magonov, B. Ozturk, *Nat. Mater.* **2003**, *2*, 413.
[8] S. Weiner, H. D. Wagner, *Annu. Rev. Mater. Sci.* **1998**, *28*, 271.
[9] S. M. Liff, N. Kumar, G. H. McKinley, *Nat. Mater.* **2007**, *6*, 76.
[10] P. Podsiadlo, A. K. Kaushik, E. M. Arruda, A. M. Waas, B. S. Shim, J. Xu, H. Nandivada, B. G. Pumplin, J. Lahann, A. Ramamoorthy, N. A. Kotov, *Science* **2007**, *318*, 80.
[11] H. D. Wagner, *Nat. Nanotechnol.* **2007**, *2*, 742.
[12] L. J. Bonderer, A. R. Studart, L. J. Gauckler, *Science* **2008**, *319*, 1069.
[13] R. A. Vaia, H. D. Wagner, *Mater. Today* **2004**, *7*, 32.
[14] P. C. LeBaron, Z. Wang, T. J. Pinnavaia, *Appl. Clay Sci.* **1999**, *15*, 11.
[15] S. S. Ray, M. Bousmina, *Prog. Mater. Sci.* **2005**, *50*, 962.
[16] E. P. Giannelis, *Adv. Mater.* **1996**, *8*, 29.
[17] M. Alexandre, P. Dubois, *Mater. Sci. Eng, R* **2000**, *28*, 1.
[18] R. A. Hule, D. J. Pochan, *MRS Bull.* **2007**, *32*, 354.
[19] C. Zilg, R. Thomann, R. Mülhaupt, J. Finter, *Adv. Mater.* **1999**, *11*, 49.
[20] C. Y. Yue, G. X. Sui, H. C. Looi, *Compos. Sci. Technol.* **2000**, *60*, 421.
[21] C. K. Ober, *Science* **2000**, *288*, 448.
[22] J. A. Disegi, L. Eschbach, *Injury* **2000**, *31*, D2.
[23] G. Decher, *Science* **1997**, *277*, 1232.
[24] A. Dundigalla, S. Lin-Gibson, V. Ferreiro, M. M. Malwitz, G. Schmidt, *Macromol. Rapid Commun.* **2005**, *26*, 143.
[25] E. Carlisle, *Calcif. Tissue Int.* **1981**, *33*, 27.
[26] E. M. Carlisle, W. F. Alpenfels, *Fed. Proc.* **1980**, *39*, 787.
[27] T. J. Gao, H. T. Aro, H. Ylanen, E. Vuorio, *Biomaterials* **2001**, *22*, 1475.
[28] I. D. Xynos, A. J. Edgar, L. D. K. Buttery, L. L. Hench, J. M. Polak, *J. Biomed. Mater. Res, Part A* **2001**, *55*, 151.
[29] E. Loizou, P. Butler, L. Porcar, E. Kesselman, Y. Talmon, A. Dundigalla, G. Schmidt, *Macromolecules* **2005**, *38*, 2047.
[30] E. Loizou, P. Butler, L. Porcar, G. Schmidt, *Macromolecules* **2006**, *39*, 1614.
[31] E. A. Stefanescu, A. Dundigalla, V. Ferreiro, E. Loizou, L. Porcar, I. Negulescu, J. Garno, G. Schmidt, *Phys. Chem. Chem. Phys.* **2006**, *8*, 1739.
[32] E. A. Stefanescu, P. J. Schexnailder, A. Dundigalla, I. I. Negulescu, G. Schmidt, *Polymer* **2006**, *47*, 7339.
[33] A. Bafna, G. Beaucage, F. Mirabella, S. Mehta, *Polymer* **2003**, *44*, 1103.
[34] Y. H. Ha, Y. Kwon, T. Breiner, E. P. Chan, T. Tzianetopoulou, R. E. Cohen, M. C. Boyce, E. L. Thomas, *Macromolecules* **2005**, *38*, 5170.
[35] H. Wang, J. K. Keum, A. Hiltner, E. Baer, B. Freeman, A. Rozanski, A. Galeski, *Science* **2009**, *323*, 757.
[36] Y. Takahashi, H. Tadokoro, *Macromolecules* **1973**, *6*, 672.
[37] L. Zhu, S. Z. D. Cheng, B. H. Calhoun, Q. Ge, R. P. Quirk, E. L. Thomas, B. S. Hsiao, F. Yeh, B. Lotz, *J. Am. Chem. Soc.* **2000**, *122*, 5957.
[38] J. M. Harris, *Poly(ethylene glycol) Chemistry: Biotechnical and Biomedical Applications*, Plenum Press, New York **1992**.
[39] K. Schwarz, *Proc. Natl. Acad. Sci. USA* **1973**, *70*, 1608.
[40] K. Schwarz, D. B. Milne, *Nature* **1972**, *239*, 333.
[41] L. L. Hench, H. A. Paschall, *J. Biomed. Mater. Res, Part A* **1973**, *7*, 25.
[42] W. Helen, C. L. R. Merry, J. J. Blaker, J. E. Gough, *Biomaterials* **2007**, *28*, 2010.
[43] D. W. Thompson, J. T. Butterworth, *J. Colloid Interface Sci.* **1992**, *151*, 236.
[44] V. Castelletto, I. A. Ansari, I. W. Hamley, *Macromolecules* **2003**, *36*, 1694.
[45] A. W. Hayes, *Principles and Methods of Toxicology*, Raven Press, New York **1994**.